

A solution-processed 1.53 μm quantum dot laser with temperature-invariant emission wavelength

S. Hoogland, V. Sukhovatkin, I. Howard, S. Cauchi, L. Levina, E. H. Sargent

*The Edward S. Rogers Sr. Department of Electrical and Computer Engineering
University of Toronto
Toronto, ON, Canada, M5S 3G4*

Sjoerd.Hoogland@utoronto.ca; Ted.Sargent@utoronto.ca

Abstract: Sources of coherent, monochromatic short-wavelength infrared (1-2 μm) light are essential in telecommunications, biomedical diagnosis, and optical sensing. Today's semiconductor lasers are made by epitaxial growth on a lattice-matched single-crystal substrate. This strategy is incompatible with direct growth on silicon. Colloidal quantum dots synthesized in solution can, in contrast, be coated onto any surface. Here we show a 1.53 μm laser fabricated using a remarkably simple process: dipping a glass capillary into a colloidal suspension of semiconductor quantum dots. We developed the procedures to produce a smooth, low-scattering-loss film inside the capillary, resulting in a whispering gallery mode laser with a well-defined threshold. While there exist three prior reports of optical gain in infrared-emitting colloidal quantum dots [1, 2, 3], this work represents the first report of an infrared laser made using solution processing. We also report $d\lambda_{\text{max}}/dT$, the temperature-sensitivity of lasing wavelength, of 0.03 nm/K, the lowest ever reported in a colloidal quantum dot system and 10 times lower than in traditional semiconductor quantum wells.

©2006 Optical Society of America

OCIS codes: (140.5960) Semiconductor lasers; (160.3380) Laser materials; (999.999) Nanocrystal quantum dots.

References and links

1. R. D. Schaller, M. A. Petruschka, and V. I. Klimov, "Tunable near-infrared optical gain and amplified spontaneous emission using PbSe nanocrystals," *J. Phys. Chem. B* **107**, 13765-13768 (2003).
2. V. Sukhovatkin, S. Musikhin, I. Gorelikov, S. Cauchi, L. Bakueva, E. Kumacheva, and E. H. Sargent, "Room-temperature amplified spontaneous emission at 1300 nm in solution-processed PbS quantum-dot films," *Opt. Lett.* **30**, 171-173 (2005).
3. G. Chen, R. Rapaport, D. T. Fuchs, L. Lucas, A. J. Lovinger, S. Vilan, A. Aharoni, and U. Banin, "Optical gain from InAs nanocrystal quantum dots in a polymer matrix," *Appl. Phys. Lett.* **87**, 251108-251110 (2005).
4. S. Kim, Y. T. Lim, E. G. Soltész, A. M. De Grand, J. Lee, A. Nakayama, J. A. Parker, T. Mihaljevic, R. G. Laurence, D. M. Dor, L. H. Cohn, M. G. Bawendi, and J. V. Frangioni, "Near-infrared fluorescent type II quantum dots for sentinel lymph node mapping," *Nat. Biotechnol.* **22**, 93-97 (2004).
5. C. J. Karlsson, F. A. A. Olsson, D. Letalick, M. Harris, "All-fiber multifunction continuous-wave coherent laser radar at 1.55 μm for range, speed, vibration, and wind measurements," *Appl. Opt.* **39**, 3716-3726 (2000).
6. L. A. Coldren and S. W. Corzine, *Diode Lasers & Photonic Integrated Circuit* (John Wiley & Sons Inc., 1995).
7. E. H. Sargent, "Infrared quantum dots," *Adv. Mater.* **17**, 515-522 (2005).
8. H. S. Rong, A. Liu, R. Jones, O. Cohen, D. Hak, R. Nicolaescu, A. Fang, and M. Paniccia, "An all-silicon Raman laser," *Nature* **433**, 292-294 (2005).
9. V. I. Klimov, A. A. Mikhailovsky, S. Xu, A. Malko, J. A. Hollingsworth, C. A. Leatherdale, H. J. Eisler, M. G. Bawendi, "Optical gain and stimulated emission in nanocrystal quantum dots," *Science* **290**, 314-317 (2000).
10. H. J. Eisler, V. C. Sundar, M. G. Bawendi, M. Walsh, H. I. Smith, and V. I. Klimov, "Color-selective semiconductor nanocrystal laser," *Appl. Phys. Lett.* **80**, 4614-4616 (2002).

11. K. Wundke, J. Auxier, A. Schulzgen, N. Peyghambarian, and N. F. Borelli, "Room-temperature gain at 1.3 μm in PbS-doped glasses," *Appl. Phys. Lett.* **75**, 3060-3062 (1999).
12. F. W. Wise, "Lead salt quantum dots: the limit of strong quantum confinement," *Acc. Chem. Res.* **33**, 773-780 (2000).
13. M. A. Hines, and G. D. Scholes, "Colloidal PbS nanocrystals with size-tunable near-infrared emission: observation of post-synthesis self-narrowing of the particle size distribution," *Adv. Mater.* **15**, 1844-1849 (2003)
14. V. I. Klimov, C. J. Schwarz, D. W. McBranch, C. A. Leatherdale, M. G. Bawendi, "Ultrafast dynamics of inter- and intraband transitions in semiconductor nanocrystals: implications for quantum-dot lasers," *Phys. Rev. B* **60**, R2177-R2180 (1999).
15. D. W. Vernooy, V. S. Ilchenko, H. Mabuchi, E. W. Streed, and H. J. Kimble, "High-Q measurements of fused-silica microspheres in the near infrared," *Opt. Lett.* **23**, 247-249 (1998).
16. G. Rempe, R. J. Thompson, H. J. Kimble, and R. Lalezari, "Measurement of ultralow losses in an optical interferometer," *Opt. Lett.*, **17**, 363-365 (1992).
17. V. R. Almeida, C. A. Barrios, R. R. Panepucci and M. Lipson, "All-optical control of light on a silicon chip," *Nature* **431**, 1081-1083 (2004).
18. J. Valenta, I. Pelant, and J. Linnros, "Waveguiding effects in the measurement of optical gain in a layer of Si nanocrystals," *Appl. Phys. Lett.* **81**, 1396-1398 (2002).
19. V. I. Klimov, A. A. Mikhailovsky, D. W. McBranch, C. A. Leatherdale, M. G. Bawendi, "Quantization of multiparticle Auger rates in semiconductor quantum dots," *Science* **287**, 1011-1013 (2000).
20. J. D. Thomson, H. D. Summers, P. M. Smowton, E. Herrmann, P. Blood, M. Hopkinson, "Temperature dependence of the lasing wavelength of InGaAs quantum dot lasers," *J. Appl. Phys.* **90**, 4859-4861 (2001).

1. Introduction

Semiconductor lasers are widely employed throughout telecommunications, information storage, medical diagnostics [4], and remote sensing [5]. Gain is provided in these devices using quantum wells, wherein electrons and holes are confined along one axis, yielding a step-like density of states. By creating a sharper joint density of states [6], quantum confinement contributes to improving the temperature stability of such lasers and lowers their laser thresholds.

Confining carriers in additional dimensions, resulting in quantum wires (2D) and quantum dots (3D), further concentrates the density of states at the band edge. In quantum dots, atomic-like states spaced by much more than the thermal energy kT should produce a peak gain wavelength which does not depend on kT , thus producing a laser whose emission wavelength depends only very weakly on temperature. Additionally, since the ground state energy and level spacing depend on quantum dot diameter, a single materials system can in principle be tuned, through control over dot diameter, to produce luminescence and gain at a range of selected wavelengths.

Quantum dots grown epitaxially using III-V compound semiconductor materials generally have large diameters compared to the Bohr exciton diameter. As a result, their atom-like states are closely spaced, standing in the way of producing a temperature-insensitive lasing wavelength, and militating against significant size-effect tuning. Additionally, epitaxial growth necessitates high temperatures, the use of dangerous gases such as arsine, and relies on a very specific choice of lattice mismatch relative to the substrate that is highly restrictive with respect to direct-growth on silicon.

In contrast, colloidal quantum dots have been synthesized with excellent monodispersity ($< 5\%$) over average diameters ranging from 1 to 10 nm. Small-radius dots exhibit very strong quantum confinement, producing levels spaced by hundreds of meV, much greater than kT at room temperature. In the PbS materials system, for example, controlled variation in colloidal dot diameter from 1 to 10 nm produces excitonic absorption peaks tunable between 850 nm and 1800 nm [7]. Colloidal nanocrystals are - in stark contrast with epitaxially-grown semiconductors-solution-processable. They are thus compatible with a wide range of substrates from crystalline to amorphous, rigid to flexible. Integration with silicon microphotonic components, for example, provides a natural route to monolithic integration of high-performance electronic and photonic components [8].

Optical gain [9] and lasing operation [10] from colloidal quantum dots have been demonstrated in visible light-emitting materials systems. Infrared gain has been shown in quantum dot nanocrystals [1, 2, 3, 11]. However, lasing has never previously been reported in such systems. PbS and PbSe, lead-salt quantum dots employed in previous reports of infrared gain, both exhibit symmetric energy band structures [12] with an 8-fold degeneracy of the first excited state. Four excitons are therefore needed to give rise to population inversion, compared to only one exciton in the CdSe systems. As a further challenge, Auger recombination, in which an electron-hole pair recombines non-radiatively with the energy transferred to a third particle, increases exponentially with decreasing bandgap. Therefore, in the lead-salt systems Auger recombination is expected to be very efficient compared to larger-bandgap systems such as CdSe.

In the present work, we first sought to find process conditions that resulted in optical gain in colloidal quantum dots. We then fabricated films from these materials and identified process conditions that resulted in sufficiently low-loss waveguides. Only then did we fabricate whispering gallery mode structures which combined gain and feedback. In these structures we observed a sharp pump power threshold and the corresponding emergence of a sharp spectral line at 1.53 μm . This work represents the first report of infrared lasing from solution-processed materials.

2. Optimization of colloidal quantum dots to achieve infrared optical gain

Figure 1 illustrates the challenges associated with achieving lasing in the infrared materials system chosen and suggests a strategy for facing these challenges. Our PbS nanoparticles were synthesized according to Ref. 13 and dispersed in hexane. As synthesized, the nanoparticles were capped with oleic acid ligands. The linear absorption spectrum exhibits [Fig. 1(a) bottom] an excitonic peak at 1480 nm (1S electron-hole transition) and 1P transition at 1000 nm. When the nanocrystals are optically pumped high above the bandgap, photoluminescence appears at about 60 nm red-shifted with respect to the 1S absorption peak. The photoluminescence quantum efficiency of this nanocrystal solution was estimated to be 30%. Carrier dynamics in the PbS nanocrystals were investigated using transient absorption measurements. The nanocrystal solution was excited using 2 ps pulses (1 kHz, 800 nm) and probed using 2 ps pulses from a continuously-tunable infrared optical parametric amplifier. Following excitation, the carriers relax such that they bleach the 1S transition within the 3 ps time-resolution of the experimental setup. The carriers subsequently recombine through Auger processes with a typical time constant of tens of picosecond and on longer timescales through radiative recombination. Unlike in CdSe nanocrystal systems [14], no photoinduced absorption was observed. The 0.8 eV photon energy of interest in this work does not, therefore, excite band-to-continuum transitions in the PbS materials system, in contrast with the 2 eV photon energy used in CdSe.

Transparency is reached when the absorption change, $\Delta\alpha$, equals the linear absorption α_0 . We fixed the delay between pump and probe to 2 ps and varied the pump power, and investigated a number of probe wavelengths in the vicinity of the 1S excitonic and photoluminescence emission peaks. We employed a wobbler to minimize local heating. The relative change in absorption increases linearly at small pump fluences and begins to saturate at about 1.2 mJ/cm^2 [Fig. 1(b)]. While the absorption at the 1S excitonic peak does not reach transparency, the absorption at 1570 nm turns into gain at a pump threshold of 7.8 mJ/cm^2 . At this wavelength the absorption of hexane has a minimum value [Fig. 1(a) top]. Gain was also observed on the low energy side of the photoluminescence peak [1] in the case of PbSe in hexane. From the saturated gain value of 7% at 1570 nm an optical gain coefficient of $\sim 5 \times 10^{-4} \text{ cm}^{-1}$ can be estimated for this nanocrystal/hexane solution. This value is a lower limit for the gain coefficient of nanocrystals in solution since hexane absorption not only increases the transparency threshold, but also reduces the measured gain values. Extrapolating the gain percentage to solid nanocrystal thin films, in which the linear absorption can reach magnitudes of hundreds inverse centimeter, a gain coefficient of tens inverse centimeter can be expected.

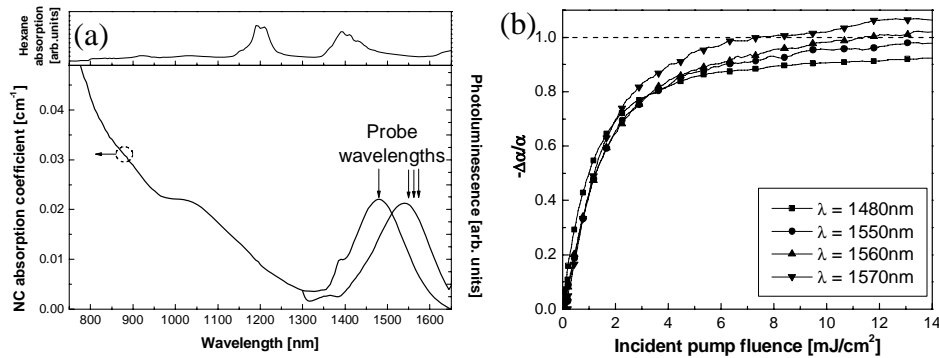


Fig. 1. (a) Room temperature absorption and photoluminescence spectrum of PbS nanocrystals in a hexane solution (bottom) and absorption spectrum of hexane (top). (b) Pump power dependence of normalized absorption changes ($-\Delta\alpha/\alpha_0$) measured at the exciton absorption peak and on the red side of the photoluminescence peak as indicated in Fig. 1(a). At 1570 nm, where there is a minimum in the hexane absorption spectrum, the relative absorption change becomes larger than 1 for a pump fluence of 7.8 mJ/cm² and optical gain is obtained.

3. Identification of conditions needed to achieve net modal gain

We observed a modest degree of population inversion. This led to two crucial conclusions with respect to the design of a laser and the minimization of its threshold fluence:

- 1) It would be essential to maximize the density of quantum dots per unit volume in order to maximize the material gain of the system for a given level of inversion. We therefore pursued a strategy based purely on quantum dots with no matrix. We also developed a procedure to replace long oleic acid ligands with short butylamine ligands to enable a maximum of close packing. In this way, we increased the packing fraction from less than 20% (oleic acid) to more than 30% (butylamine).
- 2) It would be necessary to minimize the surface roughness of quantum dot films. We developed process conditions, based on the choice of solvent, the nanoparticles' surface ligands, and the concentration of the nanoparticles in solution, aimed at producing smooth films, and monitored waveguide losses as a function of these processing conditions. We therefore aimed to achieve scattering losses less than 10 cm⁻¹, based on our estimate of the material gain achievable in a highly-packed nanocrystals thin film experiencing a modest degree of inversion.

It would be necessary to use a high-Q cavity to maximize the photon lifetime and reduce the laser build-up time and threshold fluence. Ring cavities have shown quality factors of more than 10⁹ [15] which are several orders of magnitude higher than Fabry-Perot cavities [16]. In a ring cavity whispering gallery modes (WGMs) propagate around the outer edge of a high index material (nanocrystal film) through total internal reflection, with some of their modal energy extending into the low index outer material (glass) (see Fig. 3(a) for a schematic drawing). If a thin film is used as the high-index medium, the propagating mode will be confined by not only the interface between the nanocrystals and glass but also by the interface between the nanocrystals and the inner medium (air). Therefore, not only scattering losses inside the thin film and bend losses due to the curvature of the ring resonator, but also scattering losses from the nanocrystal-air interface could reduce the ring cavity's Q-factor. Microrings can be patterned on silicon substrates in close vicinity to a microfabricated waveguide [17]. Light within the ring is subsequently amplified by the nanocrystals that fill the inner part of the ring and efficiently coupled to the waveguide through evanescent wave coupling, thus generating CMOS compatible coherent light in a waveguide.

4. Fabrication and characterization of optical waveguide made from solid thin films of pure quantum dots

To monitor scattering loss, we employed the shifting excitation spot (SES) technique [18] for which the experimental setup is schematically shown in Fig. 2(a). Here, the waveguided photoluminescence, generated by a small excitation spot that moves across the thin film, is described by the Lambert-Beer law. The 1.14 μm thick nanocrystal film was created by spin-coating a chloroform solution of butylamine-capped nanocrystals onto a substrate of 5 μm thermal oxide on silicon. In this configuration, the generated photoluminescence is confined inside the nanocrystal film since its refractive index is 1.7-1.85 compared to ~ 1.5 for the thermal oxide, whose thickness is large enough to avoid evanescent leakage into the silicon substrate. In addition to the increased packing fraction, butylamine-capped nanocrystals have the advantage of producing thick films (up to several microns) of high optical quality with a surface roughness of less than 10 nm as measured with an atomic force microscope. A sharp edge was created by cleaving the sample in half. Scanning electron microscope images of similar samples revealed that the cleaved edge propagated through the height of the nanocrystal slab waveguide, creating a relative smooth edge. The best quality edge was chosen by employing a high magnifying infrared camera that identified regions with lowest scattering intensity.

As a function of distance from the edge, the blue side of the photoluminescence peak is absorbed [(Fig. 2(b)], while the intensity at the far red side, where there is no nanocrystal absorption, is near constant. The photoluminescence intensity as function of the distance of the excitation spot from the edge reveals a single exponential decay [Fig. 2(c)] from which the absorption coefficient is obtained. At shorter wavelengths the absorption coefficient obtained from the SES data does not correspond to the values obtained in transmission measurements [Fig. 2(d)] due to the resolution of the SES experiment. However, at longer wavelengths the values do agree with each other and reveal a waveguiding loss of less than 10 cm^{-1} . This loss figure is not influenced by scattering from the imperfect cleaved edge. Losses from Rayleigh scattering due to the $\sim 4.5\text{ nm}$ diameter PbS nanocrystals were calculated to be less than 1 cm^{-1} , thus indicating that scattering losses from the nanocrystal-air and nanocrystal-thermal oxide interfaces are the main contributors to the waveguide losses. Therefore, to realize a nanocrystal laser it is imperative to ensure high quality interfaces.

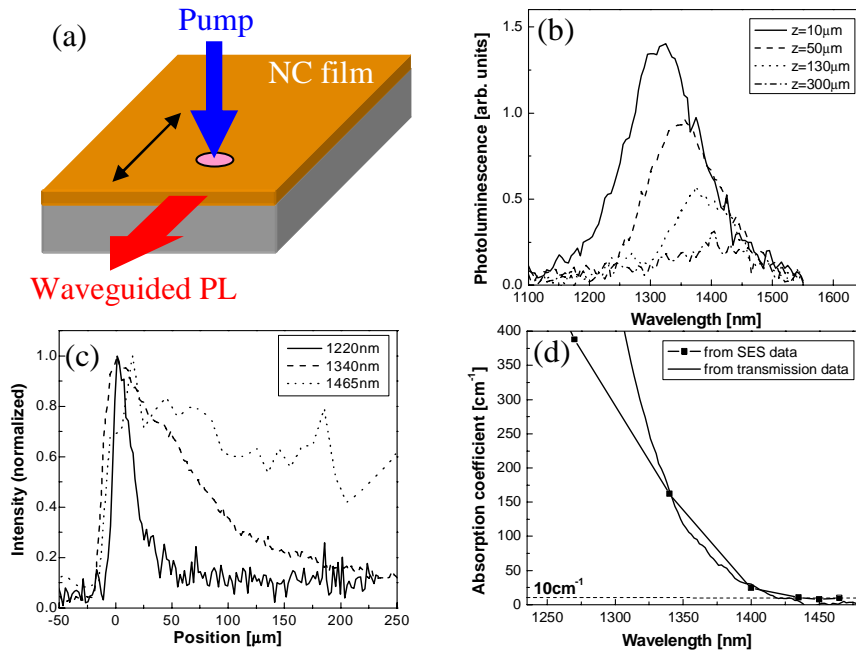


Fig. 2. (a) Schematic drawing of the Shifting Excitation Spot (SES) setup, in which the position of the pump spot on the nanocrystal (NC) film is shifted with respect to the edge of the sample from where the photoluminescence (PL) is collected (b) Guided photoluminescence spectra of a 1.14 μm thick butylamine-capped PbS nanocrystal film, when pumped at various distances, z , from the sample edge (c) Change in guided photoluminescence intensity as a function of excitation spot position at wavelengths of 1220 nm, 1340 nm and 1465 nm. (d) Absorption coefficient obtained when the SES data is fit to the Lambert-Beer law. At short wavelengths the SES data is not following the absorption spectra obtained from transmission measurements due to the resolution of the setup, while at long wavelengths, where there is no nanocrystal absorption, waveguide losses of less than 10 cm^{-1} are measured.

5. Observation of lasing operation of infrared colloidal quantum dot devices

The low waveguiding losses and the presence of optical gain in PbS nanocrystal quantum dots demonstrate the feasibility of fabricating a laser. To establish lasing action, the inner wall of a fused-silica microcapillary (Polymicro Technologies; inner diameter: $75\ \mu\text{m}$) was coated with a solid thin film of butylamine-capped nanocrystals ($\sim 5.5\ \text{nm}$ diameter), by dipping the capillary into the nanocrystal solution and subsequently force the solvent to evaporate. Images from an optical microscope show that the film thickness is less than $1\ \mu\text{m}$ [Fig. 3(b)]. The capillary was mounted onto a cold finger of a liquid nitrogen cryostat with Cryocon thermal conductive grease and pumped with 2 ps pulses (1 kHz repetition rate) at 800 nm. The emitted light from the nanocrystals was collected with a 10 cm focal length lens positioned at an angle of ~ 20 degrees with respect to the incident pump beam; the collimated light was directed to a grating monochromator and detected by a liquid-nitrogen-cooled Ge detector. The thin nanocrystal coating was within 10% uniform in thickness over a length of $300\ \mu\text{m}$, confirmed by monitoring the photoluminescence efficiency when translating the capillary along its longitudinal axis.

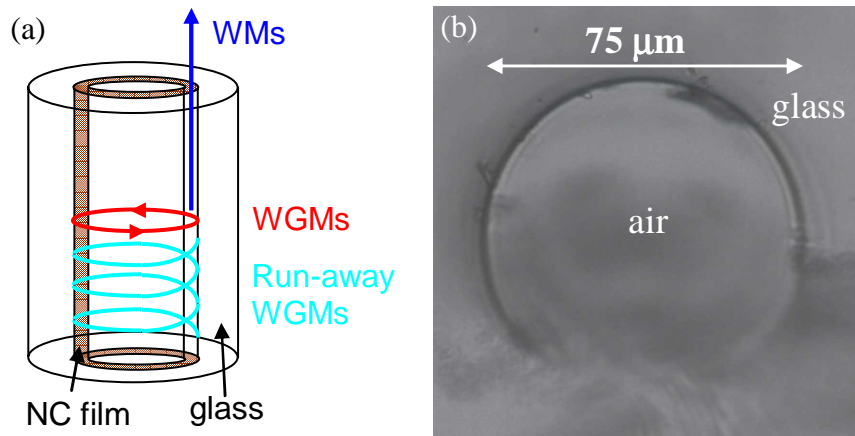


Fig. 3. (a) Schematic drawing of microcapillary tube with a solid nanocrystal thin film on the inner wall. The inner diameter of the fused silica capillary is $75\ \mu\text{m}$ and the outer diameter is $360\ \mu\text{m}$. (b) Cross-section optical microscope image of a typical microcapillary tube with a solid nanocrystal thin film on the inner wall with a width of less than $1\ \mu\text{m}$.

Upon cooling, the absorption spectrum remains essentially fixed [12], while the below-threshold photoluminescence peak red-shifts, increasing the Stokes shift to almost $200\ \text{nm}$ at $80\ \text{K}$ [Fig. 4(a)]. The emission efficiency increases as a result of an increased energy transfer rate from smaller to larger dots in which Auger processes are less efficient compared to smaller dots [19]. Energy transfer is possible since the packing fraction of butylamine capped nanocrystals is very large, ensuring exciton wavefunction overlap with more quantum dots. Also, at lower temperatures Auger recombination rates are less efficient, thus increasing the probability of energy transfer.

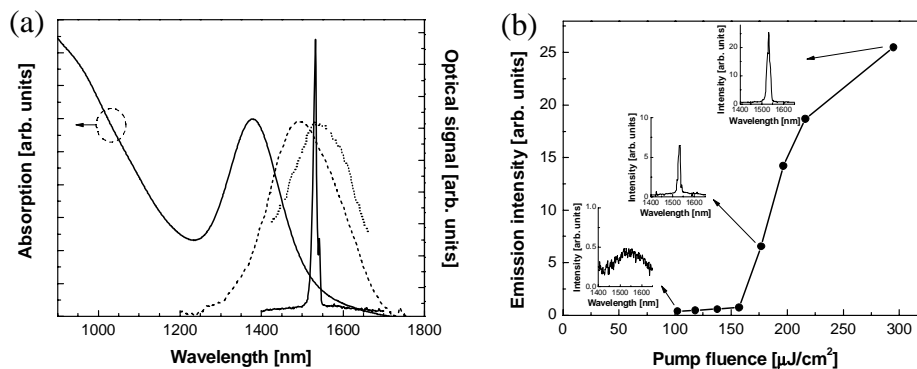


Fig. 4. (a) Absorption spectrum and normalized (below-threshold) photoluminescence spectra at room temperature (dash) and $80\ \text{K}$ (dot) of the nanocrystals used as gain medium in a $75\ \mu\text{m}$ diameter microcapillary. The increased Stokes shift at lower temperatures is a result of an increased energy transfer rate from smaller dots to larger dots. Also shown is the emission spectrum of the microcapillary laser when pumped above threshold at $80\ \text{K}$ (note the scale is made $30\times$ smaller than the photoluminescence spectrum at $80\ \text{K}$). (b) Pump fluence dependence of the nanocrystal emission from the microcapillary laser at the central lasing mode wavelength of $1532\ \text{nm}$ operating at $80\ \text{K}$. A clear sharp threshold can be observed, with a threshold fluence of $177\ \mu\text{J}/\text{cm}^2$. The insets show the emission spectra at the corresponding pump powers, clearly demonstrating the appearance of a narrow lasing peak centered at $1532\ \text{nm}$.

The photoluminescence signal of the nanocrystals linearly increases with pump fluence and eventually saturates. In different nanocrystal samples we observed neither spectral narrowing nor a nonlinear increase of the photoluminescence in the absence of optical feedback even for pump fluences in the mJ/cm^2 range. In contrast, the nanocrystals inside the capillary exhibit a clear threshold behavior at 1532 nm, where a narrow peak arises [Fig. 4(b)] at a pump fluence of $177 \mu\text{J}/\text{cm}^2$. Here, the optical gain is larger than the losses and laser oscillation commences, with a lasing wavelength that is slightly on the blue side of the low temperature photoluminescence peak [Fig. 4(a)]. A further increase of the pump fluence results in a linear increase of the lasing signal and a small increase of the lasing bandwidth (Fig. 5).

Not only do WGMs exist in the capillary, but also waveguiding modes can be supported both along the capillary and around the nanocrystal film. Only the WGMs that experience feedback can achieve true lasing action, whereas all other modes can only sustain amplified spontaneous emission. Therefore, a combination of lasing and amplified spontaneous emission is expected within the capillary when pumped above threshold. In addition, both waveguiding modes around the film and non-feedback WGMs will exhibit slight differences in mode position and spacing in the optical spectrum. Therefore, the lasing modes will not be sharply-defined as can be seen in Fig. 5. However, a mode spacing of $\sim 5.9 \text{ nm}$ can be observed, which corresponds to a modal index of ~ 1.7 . Butylamine capped nanocrystals in solid film have a refractive index of 1.7-1.85. The WGMs are therefore well-confined to the nanocrystal film. At different positions along the capillary, lasing action was observed at wavelengths varying from 1530 nm to 1560 nm, thought to be caused by non-uniformities of the nanocrystal film.

No significant hysteresis effects were observed in the laser spectrum or emission intensity as a function of pump fluence. The laser emission was stable over the course of hours, but degraded for pump fluences of more than $250 \mu\text{J}/\text{cm}^2$.

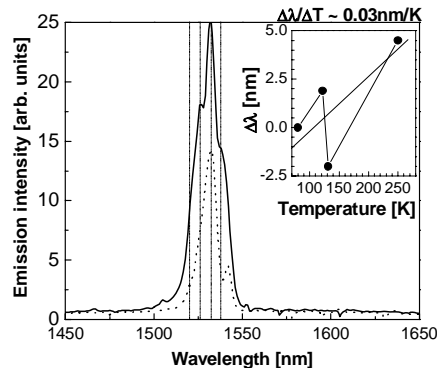


Fig. 5. Typical lasing spectrum of the PbS nanocrystal microcapillary laser at liquid nitrogen temperatures for pump fluences of $200 \mu\text{J}/\text{cm}^2$ (dotted line) and $300 \mu\text{J}/\text{cm}^2$ (solid line) displaying the increase of lasing modes with pump fluence. At a pump fluence of $300 \mu\text{J}/\text{cm}^2$, a WGM profile can be observed with a corresponding modal index of ~ 1.7 . (inset) Shift of the central lasing wavelength as function of temperature, with respect to the lasing wavelength at 80 K. An average red-shift of $0.03 \text{ nm}/\text{K}$ (solid line) can be observed from 80 K to the maximum operating temperature of 250 K.

Auger recombination and the temperature-dependence of efficient energy transfer to larger dots are expected to make the above-threshold slope of the laser emissions temperature sensitive. Increasing the temperature of the capillary subsequently resulted in a dramatic increase of the lasing threshold to several mJ/cm^2 at 250 K. No lasing action was observed above this temperature. Despite the temperature-dependence of the lasing threshold, the lasing wavelength red-shifted at an average rate of $0.03 \text{ nm}/\text{K}$ with increasing temperature (inset of

Fig. 5). This rate is 10 times smaller than the spectral shift in quantum well lasers and twice as low as in epitaxial quantum dot lasers [20].

The fast depopulation of the excited state by Auger processes limit the time of lasing operation. When the nanocrystal cavity is pumped by an ultrashort pulse, the laser ceases to oscillate as soon as the gain turns into absorption. The corresponding characteristic lasing lifetime can be obtained by a single wavelength pump-pump experiment, where each pump beam is kept below lasing threshold and the integrated lasing signal is monitored while the time-delay between the arrival of the two pump beams is varied. For a combined pump+pump power of 1.1x threshold, the lasing signal exhibits a rapid decay with a characteristic time of about 10 ps. Increasing the combined power to almost 2x threshold increases the lasing lifetime to almost 40 ps. These times are considerably longer than the ~1 ps roundtrip time of the WGMs.

6. Summary

This work presents the first solution-processed infrared laser. We first demonstrated that colloidal PbS nanocrystal quantum dots suspended in a hexane solution exhibit optical gain. In addition, solid thin films made from these nanocrystals produce waveguides with high optical quality, attested to by low waveguide losses of less than 10 cm^{-1} . These waveguides were fabricated with nanocrystals that have very short ligands to increase the packing fraction of the dots. With a decreased inter-particle spacing there is a higher probability for energy transfer from smaller to larger dots to occur. At reduced temperatures, Auger processes become less efficient and energy transfer becomes predominant, which increases the carrier population around the gain spectrum. This process step was essential to obtain whispering gallery mode lasing action around $1.55 \mu\text{m}$ from a colloidal PbS nanocrystal solid film on the inner circumference of a glass capillary. An important observation was the temperature insensitivity of the lasing wavelength over a range of 170 K. This demonstration of lasing from colloidal quantum dots in the infrared opens up the possibility of using these CMOS compatible materials in telecommunications applications. In addition, quantum information processing in the infrared can be realized once single-dot lasing can be demonstrated.